A comprehensive kinetics study on non-isothermal pyrolysis of kerogen from Green River oil shale

Wuqi Kuang[a,1], Mengke Lu[a,1], Isaac Yeboah[b], Gang Qian[a], Xuezhi Duan[a,*], Jia Yang[b], De Chen[b,*], Xinggui Zhou[a]

[a] State Key Laboratory of Chemical Engineering, East China University of Science and Technology, 130 Meilong Road, Shanghai 200237, China
[b] Department of Chemical Engineering, Norwegian University of Science and Technology, Trondheim 7491, Norway

HIGHLIGHTS

- Kerogen is prepared by extraction and decarbonation of Green River oil shale.
- Kerogen pyrolysis model is discriminated by non-linear least squares analysis.
- Two-stage model shows wide applicability to describe kerogen pyrolysis process.

ARTICLE INFO

ABSTRACT

Fundamentally understanding the pyrolysis kinetics of kerogen is of prime scientific and industrial importance. Herein, bitumen- and carbonates-free kerogen sample is prepared through Soxhlet extraction followed by decarbonation of Green River oil shale, and its pyrolysis is studied by non-isothermal thermogravimetric analysis. The systematic analyses show that both the Popescu and master plots methods are not applicable to describe the kerogen pyrolysis process due to the changed reaction model and the varied activation energy over certain conversion range, respectively, while the piecewise non-linear least squares analysis is identified as an effective method to discriminate the most probable kinetic model from commonly used 15 reaction models based on four solid-state pyrolysis mechanisms. Two-stage reaction model, i.e., F1 at the early stage and F2 at the later one, is proposed to well describe the kerogen pyrolysis process, which demonstrates a wide applicability owing to their insensitivities on the heating rate and estimation methods of the activation energies. The methodology revealed here could be applicable to determine other solid-state pyrolysis kinetics and reaction mechanism.

1. Introduction

The access to more energy is the major challenge of our time. A promising strategy to address this challenge is converting alternative hydrocarbon resources such as kerogen in oil shale to transportation fuels, which could be easily fitted into existing infrastructure. Kerogen, a sedimentary and insoluble macromolecular organic matter (OM), is by far the most abundant form of OM on Earth [1–3]. On the other hand, it has a high hydrogen-to-carbon ratio with a potential to be superior to heavy oil or coal as a source of liquid fuel [4–6].

Currently, the most common conversion technology of kerogen has been surface mining followed by thermochemical processing to produce liquid fuels (i.e., shale oil) [7,8]. To eliminate mining processes and minimize surface operations, in-situ oil shale process has been developed, which can also reduce operation cost and address environmental challenges [9,10]. For the in-situ process, a number of novel technologies like the "In-Situ Conversion Process", "Electrofrac Process", "Volumetric Heating" and "In-Situ Vapor Extraction Technology" have been developed by Royal Dutch Shell, ExxonMobil, Illinois Institute of Technology and Mountain West Energy, respectively [11–14]. The first two technologies insert resistive heaters within the formation, and utilize electric current to drive them to supply heat to the oil shale. The third one uses electrode arrays to generate radio waves to heat the formation, while the last one firstly heats methane gas above ground and then injects it into the oil-shale formation.

Considering that kerogen exists in a complicated heterogeneous mixture of organic components including bitumen linked to a mineral matrix usually containing carbonates [15–17], the thermochemical

decomposition of kerogen is usually accompanied by that of bitumen and carbonates, leading to very complex thermal behaviors. Therefore, it is highly desirable to exclude the interference of bitumen and carbonates for understanding the intrinsic thermal behavior of kerogen. Previous studies [1,18–20] demonstrated that the bitumen and carbonates can be easily removed by extraction in Soxhlet extractor with solvent like CH_2Cl_2 and conventional acid treatment without altering the kerogen, respectively.

As an effective method, pyrolysis, a process of heating materials in an inert environment, is widely employed to convert kerogen into shale oil [21,22]. This viable pyrolysis process could be complicated because kerogen has a complex chemical structure, where there are different types of heteroatoms like oxygen, nitrogen and sulfur, and different kinds of groups like ketone, carboxyl and ester [23–27]. To develop and optimize the process, it requires discriminating the pyrolysis mechanism, obtaining the kinetic triplet (i.e., activation energy, pre-exponential factor and reaction model [28]) and establishing the reaction kinetics. However, the relevant studies on kerogen pyrolysis are carried out by using oil shale with bitumen and carbonates (e.g., pyrolysis conditions [29–32] and kinetics [22,28,33–36]), and rarely by using bitumen- and carbonate-free kerogen. Previously, isoconversional methods without any assumption about reaction kinetics model have been successfully demonstrated to estimate the activation energies of kerogen pyrolysis with almost 140–240 kJ/mol [37,38]. Master plots method used for discriminating the pyrolysis kinetics model of isolated kerogen has been employed [19], but the deviation between the experimental data and calculated data seems to be high. Moreover, it is reported that transformation of hydrogen-rich organic matter like kerogen to oil and gas can be described by (near) first-order kinetics, where the activation energy for the whole process is a single value regardless of any possible variation along the conversion range [33,39]. Therefore, these is a need to carry out a comprehensive and in-depth kinetics study for kerogen pyrolysis.

Thermogravimetric analysis (TGA) is extensively used for kinetics study of solid-state pyrolysis process, where there are isothermal and non-isothermal methods [40–42]. The isothermal method is carried out at a given reaction temperature, and can reflect the overall reaction characteristics of the solid. This method separates temperature effect (i.e., the reaction rate constant) and kinetic function model, thus providing a simple and reliable determination of the reaction kinetics [43,44]. However, for isothermal gas-solid reaction like char gasification in a micro fluidized bed, the effects of gas mixing and diffusion on the measured reaction will be very serious when inert gas is switched to reactant gas, only if the reaction rate is very high [45]. The non-isothermal method is conducted by exposing a sample to a programmed reaction temperature variation, which can reveal the thermal behavior under different temperatures and clarify the relationship between heating rate and reaction characteristics [43]. Comparing to the isothermal method, the non-isothermal method is simple and easy because it can avoid the change of chemical and physical properties of the tested sample, and provide useful information via fewer experiments [43,46]. Moreover, the non-isothermal method can also offer certain advantages on eliminating the errors caused by the thermal induction period and permitting a rapid scan of the whole temperature range of interest [47], which has been proved to be important in many cases like pyrolysis of biomass, water plastics and tyres [48–50]. Thus, the non-isothermal method is chosen in TGA.

Based on the obtained TGA data, there are different model-free isoconversional methods (e.g., Friedman [51], KAS [52], FWO [52,53], NL-INT [54] and NL-DIF [55]) and different kinetics model-fitting methods (e.g., Popescu method [56], master plots method [57] and non-linear least squares analysis [58–60]) to estimate the activation energies and discriminate the reaction model from various solid-state kinetic models according to their mechanistic basis as nucleation, geometrical contraction, diffusion, and reaction order [61], respectively. Comparison between the isoconversional and model-fitting

methods has been made by Burnham and Dinh [62], the results show that the two methods are applicable to reactivity distribution of parallel reactions involving complex materials, but it is still difficult to determine which method will give more accurate predictions. Notably, understanding pyrolysis behavior of a certain material requires systematic investigation and comparison by using these different methods, aiming to reveal the plausible kinetics and reaction mechanism.

In this work, bitumen- and carbonates-free kerogen was prepared through Soxhlet extraction with CH_2Cl_2 followed by decarbonation of Green River oil shale, and its non-isothermal pyrolysis was studied by TGA. Subsequently, three commonly used model-fitting methods, i.e., the Popescu method, master plots method and non-linear least squares analysis, were employed to discriminate the most probable kinetic model from the 15 reaction models based on the four types of solid-state pyrolysis mechanisms. Furthermore, the proposed two-stage reaction model was confirmed by checking the activation energies and heat flow along the entire conversion range and two-stage kinetic compensation effects, and their universality was tested by probing their applicability under different heating rates and different estimation methods of activation energies.

2. Experimental and theoretical methods

2.1. Preparation of kerogen sample

The kerogen sample was prepared through Soxhlet extraction followed by decarbonation of Green River oil shale. Specifically, the oil shale sample was crushed, homogenized and then sieved to 80 meshes (~0.2 mm) for minimizing the effects of heat and mass transfer, which could influence the decomposition rate with particle size larger than 0.4 mm [63]. The finely ground oil shale sample was treated with CH_2Cl_2 to extract the bitumen until the solvent in the Soxhlet arm becomes colorless. Subsequently, the bitumen-free oil shale was treated with 6 M HCl under nitrogen for 12 h. The resultant sample was thoroughly washed with hot distilled water, and then dried in a vacuum oven to obtain the kerogen sample.

2.2. Characterization

X-ray diffraction patterns of the oil shale and kerogen samples were recorded using a Rigaku D/Max 2550VB/PC diffractometer equipped with Cu K_α radiation ($\lambda = 1.5406$ Å). A thermogravimetric analyzer (TA Instrument SDT-Q600) was used to study the thermal behavior of the oil shale and/or kerogen samples in air and nitrogen flow atmosphere of 150 mL/min from room temperature up to 1173 K. Duplicate experiments were performed to ensure reproducibility.

2.3. Theoretical methods for determination of kinetic triplet

The non-isothermal pyrolysis kinetics of kerogen can be expressed as:

$$\frac{d\alpha}{dt} = kf(\alpha) = A\exp\left(-\frac{E}{RT}\right)f(\alpha) \tag{1}$$

where $\frac{d\alpha}{dt}$ is the conversion rate of reaction, α is the degree of conversion, k is the rate constant, $f(\alpha)$ is the conversion function depending on the reaction mechanism in Table 1 [40,61,64]. A is the pre-exponential factor (s^{-1}), E is the activation energy (kJ/mol), R is the universal gas constant and $g(\alpha)$ is the integral expression of the $f(\alpha)$. The α is a function of initial mass W_0, final mass W_∞ and mass of sample at time t (W_t):

$$\alpha = \frac{W_0 - W_t}{W_0 - W_\infty} \tag{2}$$

By substituting β (i.e, constant heating rate, dT/dt, K/min) into the Eq. (1), Eq. (3) can be also expressed as:

Table 1
Fifteen main kinetics models ($f(\alpha)$) and their integral expressions ($g(\alpha)$) of solid-state pyrolysis process.

Model	$f(\alpha)$	$g(\alpha)$
Reaction-order model		
First-order (F1)	$(1-\alpha)^1$	$-\ln(1-\alpha)$
Second-order (F2)	$(1-\alpha)^2$	$(1-\alpha)^{-1}-1$
Third-order (F3)	$(1-\alpha)^3$	$[(1-\alpha)^{-2}-1]/2$
Nucleation model		
Power law (P2)	$2\alpha^{1/2}$	$\alpha^{1/2}$
Power law (P3)	$3\alpha^{2/3}$	$\alpha^{1/3}$
Power law (P4)	$4\alpha^{3/4}$	$\alpha^{1/4}$
Avrami-Erofe've (A2)	$2(1-\alpha)[-\ln(1-\alpha)]^{1/2}$	$[-\ln(1-\alpha)]^{1/2}$
Avrami-Erofe've (A3)	$3(1-\alpha)[-\ln(1-\alpha)]^{2/3}$	$[-\ln(1-\alpha)]^{1/3}$
Avrami-Erofe've (A4)	$4(1-\alpha)[-\ln(1-\alpha)]^{3/4}$	$[-\ln(1-\alpha)]^{1/4}$
Geometrical contraction model		
Contracting area (R2)	$2(1-\alpha)^{1/2}$	$1-(1-\alpha)^{1/2}$
Contracting volume (R3)	$3(1-\alpha)^{2/3}$	$1-(1-\alpha)^{1/3}$
Diffusion model		
1-D diffusion (D1)	$1/2\alpha$	α^2
2-D diffusion (D2)	$-1/\ln(1-\alpha)$	$[(1-\alpha)\ln(1-\alpha)]+\alpha$
3-D diffusion (D3)	$3(1-\alpha)^{2/3}/[2(1-(1-\alpha)^{1/3})]$	$-[1-(1-\alpha)^{1/3}]^2$
Ginstling-Brounshtein (D4)	$3/2[(1-\alpha)^{-1/3}-1]$	$1-(2\alpha/3)-(1-\alpha)^{2/3}$

$$\frac{d\alpha}{dT} = \frac{A}{\beta}\exp\left(-\frac{E}{RT}\right)f(\alpha) \tag{3}$$

For the reaction mechanisms, they are classified into four types based on mechanistic assumptions [65]. The nucleation models assume the formation and growth of nuclei to be the rate-limiting step. The geometrical contraction models assume nucleation to be instantaneous throughout the surface and the rate-limiting step to be the progress of the product layer from the surface of the crystal inward. The diffusion models consider the diffusion of reactants into reaction sites or products away from reaction sites as the rate-limiting step, while the reaction-order models are similar to the same rate expressions in homogenous kinetics, and the rate law is based on the reaction order.

2.3.1. Determination of activation energy

The activation energy (E) can be estimated by using five main isoconversional methods, i.e., three linear Friedman, FWO and KAS together with two non-linear NL-INT and NL-DIF. The isoconversional methods can be applied to multistep reactions, and reveal a dependence of the activation energy on conversion [54]. The Friedman method uses the differential form of the rate equation (i.e, Eq. (1)) and does not need to make any mathematical approximations [66]. It employs instantaneous rate values and is sensitive to experimental noise, and thus lead to some errors, which could be reduced by the advent of software with smoothing capabilities [52]. The FWO and KAS methods use the integrated form of the rate equation, and assume constant activation energy, which could result in an associated and unavoidable error [52]. The equations of these three methods are listed in Table 2 [40], and the derivation details of the models are given in Supplementary

Table 2
Three linear isoconversional methods.

Method	Model	Y	X
Friedman	$\ln\left(\frac{d\alpha}{dt}\right)=\ln\left(\beta\frac{d\alpha}{dT}\right)=\ln[Af(\alpha)]-\frac{E}{RT}$	$\ln\left(\beta\frac{d\alpha}{dT}\right)$	$1/T$
FWO	$\ln(\beta)=\ln\left(\frac{AE}{Rg(\alpha)}\right)-5.331-1.052\frac{E}{RT}$	$\ln(\beta)$	$1/T$
KAS	$\ln\left(\frac{\beta}{T^2}\right)=\ln\left(\frac{AR}{g(\alpha)E}\right)-\frac{E}{RT}$	$\ln\left(\frac{\beta}{T^2}\right)$	$1/T$

Table 3
Two non-linear isoconversional methods.

Method	Model
NL-INT	$\left\|\sum_{i=1}^{n}\sum_{j\neq i}^{n}\frac{\beta_j I(E_\alpha,T_{\alpha,i})}{\beta_i I(E_\alpha,T_{\alpha,j})}-n(n-1)\right\|=\min$
NL-DIF	$\left\|\sum_{i=1}^{n}\sum_{j\neq i}^{n}\frac{\beta_i\left(\frac{d\alpha}{dT}\right)_i\left[\exp\left(\frac{E_\alpha}{RT_{\alpha,i}}\right)\right]}{\beta_j\left(\frac{d\alpha}{dT}\right)_j\left[\exp\left(\frac{E_\alpha}{RT_{\alpha,j}}\right)\right]}-n(n-1)\right\|=\min$

Information. Under the same value of α at different heating rates, the activation energy (E) was determined from the slope of regression lines of Y versus X.

Compared to the FWO and KAS with oversimplified approximation of temperature integral ($p(x)$, $x = E/RT$), as shown in Supplementary Information in detail, the NL-INT method is independent on x value, thus showing extremely low errors [54]. Moreover, the two non-linear methods are independent on the relationship between activation energy and conversion [55]. The non-linear methods are listed in Table 3, and the derivation details of the models are also given in Supplementary Information. For the NL-INT method, by substituting experimental values of T_α and β into the model and varying E_α to reach the minimum, it gives the value of the activation energy at a given conversion. For the NL-DIF method, by substituting experimental values of T_α, β and $d\alpha/dT$ into the model and varying E_α to reach the minimum, it gives the value of the activation energy at a given conversion.

2.3.2. Determination of kinetic model and pre-exponential factor

The most probable kinetic model can be determined by three commonly used methods, i.e., the Popescu method, master plots method and non-linear least squares analysis.

For the Popescu method, its curve fitting procedure is an integral method, which investigates kinetics and mechanism of reaction by using the degree of conversion measured at the same temperatures on curves recorded for a reaction carried out at various heating rates. Its main advantage is that it does not need any assumption concerning the temperature integral and less affected by experimental errors [67].

By using the integral form of Eq. (3), it gives

$$\int_{\alpha_m}^{\alpha_n}\frac{d\alpha}{f(\alpha)}=\frac{1}{\beta}\int_{T_m}^{T_n}k(T)dT \tag{4}$$

where α_m and α_n are two different degrees of conversion, and T_m and T_n are their corresponding temperatures. By using the notations:

$$g(\alpha)_{nm}=\int_{\alpha_m}^{\alpha_n}\frac{d\alpha}{f(\alpha)} \tag{5}$$

and

$$I(T)_{nm}=\int_{T_m}^{T_n}k(T)dT \tag{6}$$

which are the integral of conversion and temperature, respectively, the Eq. (4) can be transformed into a short form:

$$g(\alpha)_{nm}=\frac{1}{\beta}I(T)_{nm} \tag{7}$$

For two selected temperatures T_m and T_n, a pair of α (i.e., (α_{m1}, α_{n1}), (α_{m2}, α_{n2}), ...,) under different heating rates β (i.e., β_1, β_2, ...,) can be determined from the obtained experimental data. With the above pairs of T, α and β, and the various reaction models given in Table 1, the values of $g(\alpha)_{mn1}$, $g(\alpha)_{mn2}$, ... can be calculated according to Eq. (5). Since the selected temperatures T_m and T_n are respectively the same at different heating rates according to the Eq. (7), the value of I_{mn} should be constant. Thus, a linear fitting of the $g(\alpha)_{mn}$ and $1/\beta$ were performed with an intercept of zero, and the obtained coefficients of determination (R_2) can be the measures of the most probable kinetic

model [52].

For the master plots method, the experimental data are firstly transformed into an experimental master plot. Then, it is compared with theoretical master plots, which are dependent on the kinetic model, but independent on the kinetic parameters (i.e., E and A) [68], and can be drawn by assuming certain kinetic models and serve as references. Thus, the kinetic model or the general type of model can be determined by a simple graphical procedure. This method does not need to assume the kinetic model followed by the reaction, preventing errors arising from the fit to inappropriate kinetic models [68–70].

By combining Eq. (1) and the Coats-Redfern equation [71], the $g(\alpha)$ can be obtained:

$$g(\alpha) = \frac{ART^2}{E\beta}\exp\left(-\frac{E}{RT}\right) \tag{8}$$

the expression of the reduced master plots method developed by Criado [57] can be obtained:

$$y(\alpha) = \frac{f(\alpha)g(\alpha)}{f(0.5)g(0.5)} = \left(\frac{T}{T_{0.5}}\right)^2 \frac{(d\alpha/dt)}{(d\alpha/dt)_{0.5}} \tag{9}$$

where $T_{0.5}$ and $(d\alpha/dt)_{0.5}$ are the temperature and the kerogen pyrolysis rate, respectively, under the conversion (α) of 0.5. By substituting the corresponding temperature T at the selected α under different β into Eq. (9), experimental master plots of $y(\alpha)$ vs α can be drawn. Meanwhile, by substituting α values into integral kinetic mechanisms, the theoretical master plots of $y(\alpha)$ vs α can be produced [40]. If the theoretical master plots coincide with the experimental plots, the $f(\alpha)$ is chosen as the most probable kinetic model.

For the non-linear least squares analysis, optimization program is carried to match model predictions with measured data, where the error function can be used [72–74]:

$$S = \sum_{i}^{n} (y_i^{\exp} - y_i^{th})^2 \tag{10}$$

with $y_i^{\exp} = (d\alpha/dT)_{\exp}$ and $y_i^{\mathrm{fit}} = (d\alpha/dT)_{\mathrm{fit}}$

where the S is a square sum of differences between experimental and fitted data, and the $y_i^{\exp}$ and y_i^{fit} are experimental and fitting data, respectively. For each reaction model, by varying the pre-exponential factor (A) to minimize the S value when fitting the calculated data to experimental ones, the A values based on each model and the corresponding fitting curves can be obtained. If the calculated data give a good fit to the experimental data, the selected reaction model can be determined as the most probable kinetic model.

3. Results and discussion

3.1. Preparation of bitumen- and carbonates-free kerogen

Kerogen sample was prepared through Soxhlet extraction with dichloromethane followed by decarbonation of Green River oil shale, which were used to remove the bitumen and carbonates, respectively. The complete extraction of bitumen is easily guaranteed by checking whether the solvent in the thimble-holder and siphon becomes colorless. However, XRD and TGA-DSC measurements of the as-prepared kerogen sample and raw oil shale sample as a comparison were carried out to probe whether the carbonates are completely removed.

As it can be seen in Fig. 1a, dolomite, ankerite, calcite, albite and quartz-type inorganic matters are identified as the main components of the oil shale according to the standard powder diffraction cards of JCPDS. The dolomite, ankerite and calcite are carbonates, and their peak intensities dramatically decrease over the kerogen due to the decarbonation treatment. Moreover, for the TGA-DSC analyses in Fig. 1b, the oil shale sample exhibits two main low-temperature weight loss stages/peaks with exothermic characteristics arising from the

oxidation of organic matters, and one high-temperature weight loss stage/peak with endothermic nature resulting from the decomposition of the carbonates. However, for the kerogen sample, there is no legible endothermic peak, indicating almost complete removal of the carbonates. All of these results demonstrate that our prepared kerogen sample is bitumen- and carbonates-free, which would be used as the starting material for fundamental understanding of kerogen pyrolysis kinetics without the interferences from bitumen and carbonates.

3.2. Determination of optimal method to obtain the most probable model

Thermal behavior of the as-prepared kerogen sample was studied by TGA analyses at the heating rates of 2, 5, 10 and 20 K/min, and the results are shown in Fig. 2a. Based on these TGA data, we employ three commonly used methods, i.e., the Popescu method, master plots method and non-linear least squares analysis, to discriminate the most probable kinetic model from the 15 reaction kinetics models mentioned above and thus to fundamentally understand the thermal behavior of kerogen.

The Popescu method was firstly employed to determine the most probable kinetic model. It can be seen in Fig. 2b that approximately seven kinetic models, i.e., the F1, F2, R3, D1, D2, D3 and D4, exhibit relatively high coefficients of determination (R^2) values, from which it is difficult to determine the most probable kinetic model just by using the R^2. In other words, the Popescu method cannot directly lead to the most probable kinetic model, and subsequent efforts are need for the determination. This is indicates the highly insensitive characteristics of the method, demonstrating that it is not appropriate to discriminate the most probable kinetic model of the kerogen pyrolysis process. It is noted that the some R^2 values are missed, which is because the calculation cannot be executed through the Popescu method by using the P2, P3, P4 and D4 models.

Furthermore, the master plots method was employed to determine the most probable kinetic model. As shown in Fig. 2c, Fig. S1 and Table S1, three models, i.e., the F1, A3 and A4, are observed with relatively high R^2 values. It is noted that for this method, its requirement is almost constant activation energy along the entire conversion range [68]. Along this line, isoconversional kinetic analysis procedures were carried out to estimate the activation energies (E) under different degree of conversion (α), where the commonly used isoconversional methods, i.e., the Friedman, was employed. It can be obviously seen in Fig. 3a that the activation energies determined from the Friedman method exhibit a remarkably increased trend, which does not meet the above requirement. All of these results call special attention to combine the master plots method with the isoconversional method for reasonably determining the most probable kinetic model [68], despite that the combination is not applicable in our case.

As a consecutive effort, the piecewise non-linear least squares analysis was performed by using the data under the heating rate of 5 K/min with the conversion interval of less than or equal to 0.05, where the maximal change degree of the activation energies in each interval is acceptable ($< 5\mathrm{kJ/mol}$) and their values under different conversions are shown in Table S2. The comparisons between the experimental data and the fitting data by using the 15 reaction models based on the activation energies from the Friedman method are shown in Fig. 3b and Fig. S2. According to these visual interpretations and the corresponding R^2 values listed in Table S3, it is concluded that the kerogen pyrolysis almost follows F1 model (i.e., first-order reaction model) at the early stage (i.e., $\alpha = 0$–0.9), and then the F2 model (i.e., second-order reaction model) at the late one (i.e., $\alpha = 0.9$–1.0). In other words, the kerogen pyrolysis follows the two-stage reaction model. According to previous studies [31,75,76], the first stage reaction model is most likely attributed to the cracking of kerogen and its pyrolytic bitumen, and the second stage one to the polymerization and condensation of some pyrolytic products to form residual carbon and coke.

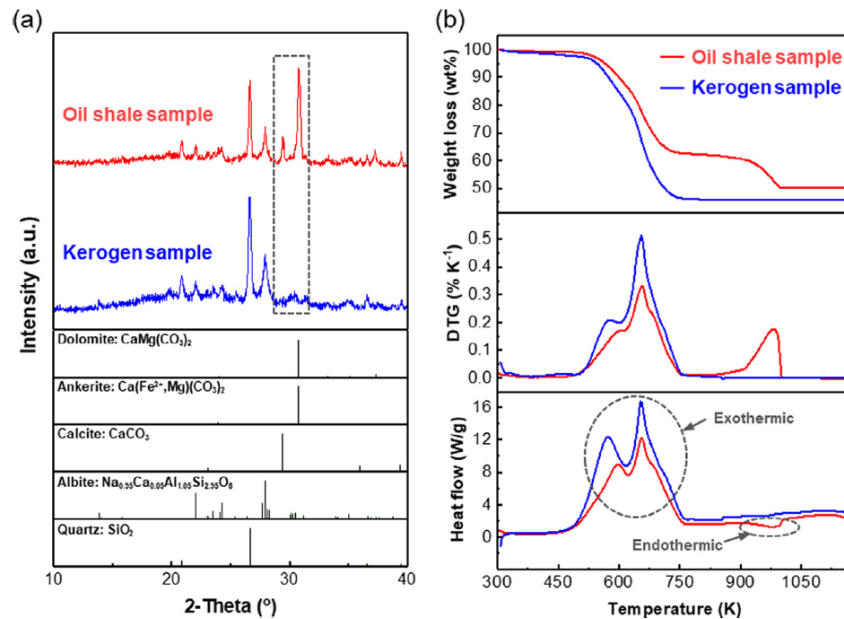It is noted that the two-stage reaction model provides an

Fig. 1. (a) XRD patterns and (b) TGA-DSC profiles of raw oil shale sample and as-prepared kerogen sample. [The standard powder diffraction cards of quartz (PDF#85-0795), albite (PDF#70-3752), ankerite (PDF#41-0586), calcite (PDF#83-0577) and dolomite (PDF#73-2409) are also presented.]
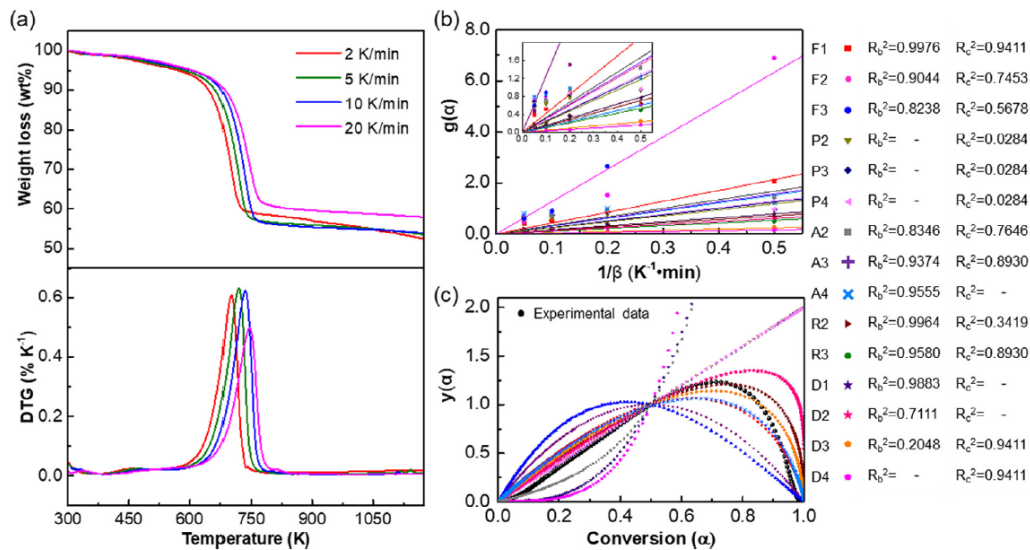

Fig. 2. (a) TGA/DTG profiles of kerogen pyrolysis under different heating rates; (b) Fitting curves for different kinetic models based on the Popescu method; (c) Theoretical and experimental (5 K/min) master plots for different kinetic models based on the master plots method.

explanation for the infeasibility of Popescu method to determine the reaction model because of its assumption of unchanged reaction model over certain conversion range [56]. Moreover, the piecewise non-linear least squares analysis is demonstrated to be appropriate to determine the reaction model of kerogen pyrolysis, which could avoid the errors from the sharp/unacceptable change of activation energy and the change of reaction model over the conversion range.

3.3. Mechanism behind the two-stage reaction model

To understand the above issues, the activation energies (Fig. 3a) and heat flow along the entire conversion range, as shown in Fig. 4a, were analyzed discussed. Typically, four obvious stages of activation energies in the kerogen pyrolysis process are observed. Specifically, at the first stage ($0 \leq \alpha \leq 0.06$), the low activation energies are most likely due to cracking of the weak chemical bonds in kerogen to a small amount of gas (mainly H_2O, CO_2, H_2S and light hydrocarbon) [77], which is consistent with weak DSC peaks at around 625 K, and its decreased
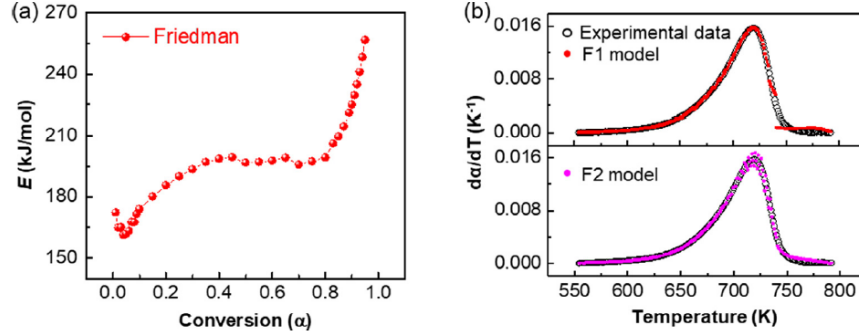
Fig. 3. (a) Relationships between activation energy (E) and conversion (α) calculated by the Friedman methods; (b) Comparisons between experimental data and the fitting data by using the F1 and F2 models based on activation energies from the Friedman.
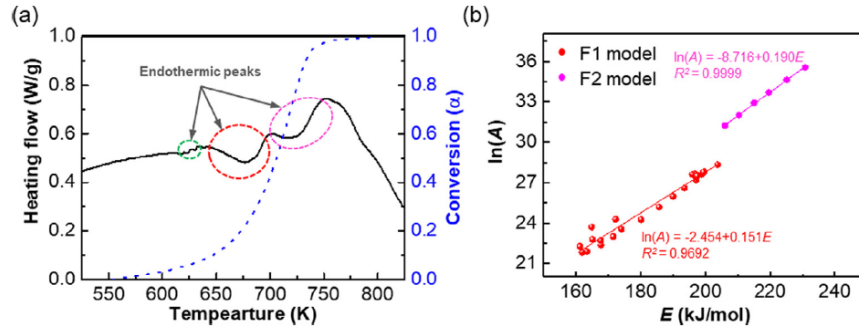

Fig. 4. (a) DSC profile and conversion (α) versus kerogen pyrolysis temperature under heating rate of 5 K/min; (b) Kinetic compensation effect for the non-isothermal pyrolysis kinetics of kerogen.

trend might arise from the promoted cracking by the resultant H_2O/CO_2. At the second stage ($0.06 \leq \alpha \leq 0.40$), the increased activation energies could be owing to the stepwise decomposition of kerogen to bitumen [75], and the weight loss of the sample in principle results from the conversion of the pyrolytic bitumen to gas and aliphatic oil, where these processes lead to a strong endothermic DSC peak at approximate 650–700 K. At the third stage ($0.40 \leq \alpha \leq 0.80$), the relatively stable activation energies could be associated with the cracking of bitumen and its pyrolytic products [75]. At the last stage ($0.80 \leq \alpha \leq 1.00$), the increased activation energies may arise from the polymerization and condensation of some pyrolytic products to form residual carbon and coke [75]. The last two stages correspond to another strong endothermic DSC peak at approximate 700–750 K. These analyses could explain why the kerogen pyrolysis process can be well described by combining the F1 with F2 reaction models.

Subsequently, $\ln(A)$ is respectively plotted with E in the conversion range of 0–0.9 and 0.9–1.0 to probe whether there exist two-stage kinetic compensation effects, which is a way to demonstrate that the pyrolysis process is correctly described by the selected model [47]. It should be pointed out that the used E values at different conversion ranges are listed in Table S2, and the corresponding A values were obtained by the combination of non-linear least squares analysis and reaction models, as also shown in Table S2. As expected, there are two linear relationships between the $\ln(A)$ and E in Fig. 4b, indicating the existence of two-stage kinetic compensation effects [78]. This further confirms the above proposed two-stage reaction model for the kerogen pyrolysis. Therefore, the non-isothermal pyrolysis kinetics of kerogen can be expressed as:

$$\frac{d\alpha_i}{dT_{\alpha,i}} = \frac{A_{\alpha,i}}{\beta} \exp\left(-\frac{E_{\alpha,i}}{RT_{\alpha,i}}\right) f(\alpha) \tag{11}$$

with

$f(\alpha) = (1 - \alpha)$(i.e. , F1 reaction model) for $0 \leq \alpha \leq 0.9$,

$f(\alpha) = (1 - \alpha)$(i.e. , F2 reaction model) for $0.9 \leq \alpha \leq 1.0$,

where the $E_{\alpha,i}$ and A_i values under different conversions are shown in Table S2.

3.4. Practicability of the two-stage reaction model

Moreover, our proposed two-stage reaction model was also applied for the kerogen pyrolysis under other three heating rates, i.e., 2, 10 and 20 K/min, where the E and A values at different conversion ranges for each heating rate are obtained by the same method as above, i.e., the Friedman method and the non-linear least squares analysis. It is shown in Fig. 5 that for the three cases, the two-stage reaction model can give good fits of the kerogen pyrolysis profiles, indicating the practicability of the proposed two-stage reaction model for different heating rates.

Based on the above systematic analyses, the Popescu method and master plots method are found to be not applicable for describing the TGA data of kerogen pyrolysis, while the non-linear least squares analysis is identified as an effective method to discriminate the most probable kinetic model from the commonly used 15 reaction models based on the four types of solid-state pyrolysis mechanisms. It is noted that the non-linear least squares analysis is only based on the estimated activation energies by the Friedman isoconversional method. Considering that other isoconversional methods are widely used to estimate the activation energies [79], the four commonly used methods, i.e., the FWO, KAS, NL-INT and NL-DIF, were also employed for estimating the activation energies of the kerogen pyrolysis. As shown in Fig. 6a, the four isoconversional methods give similar trends of the activation energies along the entire conversion range compared to the
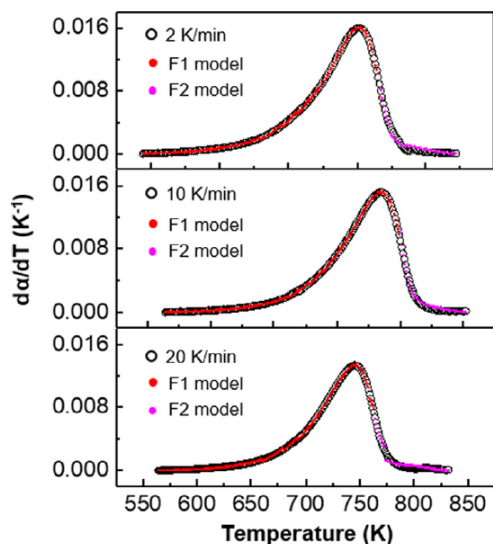
Fig. 5. Comparisons between experimental data and the fitting data by using the F1 and F2 models under different heating rates.

Friedman method. Based on these estimated activation energies, we employed the optimal non-linear least squares analysis and the proposed two-stage reaction model to probe whether the kerogen pyrolysis process can be well described. As expected, that the calculated data based on the four methods show good fits to the TGA data, as shown in Fig. 6b. This indicates an insensitivity of the proposed two-stage

reaction model for the kerogen pyrolysis process on the estimation methods of the activation energies. In other words, the proposed two-stage reaction model has a wide applicability for describing the kerogen pyrolysis process.

4. Conclusions

In summary, we have proposed the kinetics and reaction mechanism of the non-isothermal pyrolysis of kerogen prepared through Soxhlet extraction followed by decarbonation of Green River oil shale. Both the Popescu method and master plots method are found to be not applicable to describe the kerogen pyrolysis process owning to the changed reaction model and varying activation energy over certain conversion range. The piecewise non-linear least squares analysis is identified as an effective method for the discrimination of the most probable kinetic model from the commonly used 15 reaction models based on four types of solid-state pyrolysis mechanisms because it can avoid the errors from the sharp/unacceptable change of activation energy and the change of reaction model over the conversion range. The two-stage reaction model, i.e., F1 at the early stage and F2 at the later one, is proposed to well describe the kerogen pyrolysis process, which demonstrates a wide applicability owing to their insensitivities on the heating rate and estimation methods of the activation energies. The insights reported here could guide the rational design and optimization of kerogen pyrolysis process, and the methodology could be applicable for determining other solid-state kinetics and reaction mechanism.
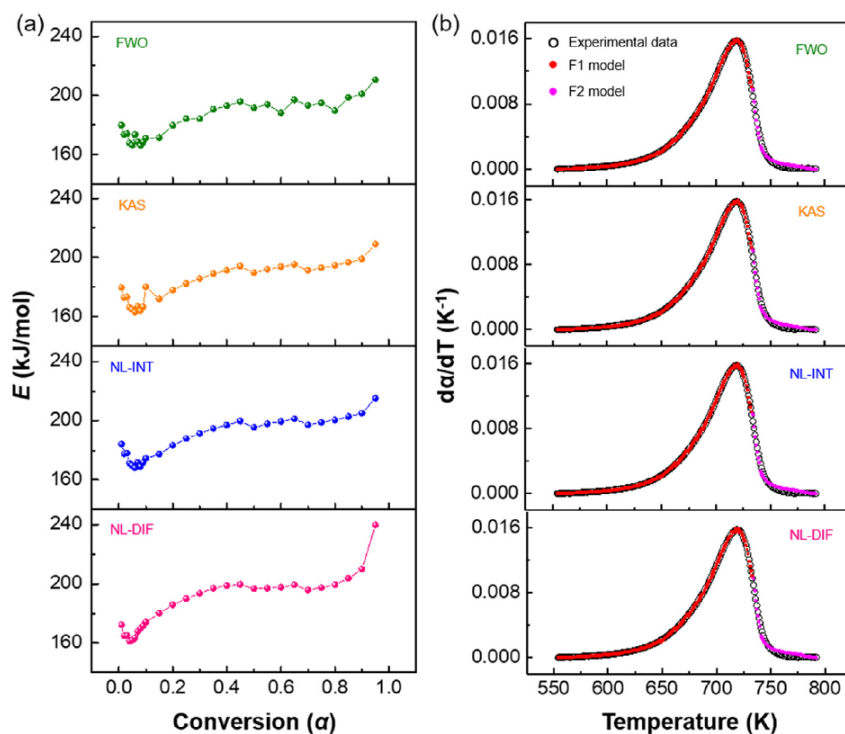
Fig. 6. (a) Activation energies estimated by the FWO, KAS, NL-INT and NL-DIF methods; (b) Comparisons between experimental data and the fitting data by using the F1 and F2 models based on activation energies estimated by the FWO, KAS, NL-INT and NL-DIF methods.

Appendix A. Supplementary data

Supplementary data to this article can be found online at https://doi.org/10.1016/j.cej.2018.10.212.

References

[1] M. Vandenbroucke, C. Largeau, Kerogen origin, evolution and structure, Org. Geochem. 38 (2007) 719–833.

[2] L. Atmani, C. Bichara, R.J.M. Pellenq, H. Van Damme, A.C. Van Duin, Z. Raza, L.A. Truflandier, A. Obliger, P.G. Kralert, F.J. Ulm, J.M. Leyssale, From cellulose to kerogen: molecular simulation of a geological process, Chem. Sci. 8 (2018) 8325–8335.

[3] D. Zhang, D. Duan, Y. Huang, Y. Yang, Y. Ran, Composition and structure of natural organic matter through advanced nuclear magnetic resonance techniques, Chem. Biol. Technol. Agric. (2017) 4–8.

[4] P.A. Bozkurt, O. Tosun, M. Canel, The synergistic effect of co-pyrolysis of oil shale and low density polyethylene mixtures and characterization of pyrolysis liquid, J. Energ. Inst. 90 (2017) 355–362.

[5] P. Biller, A.B. Ross, S.C. Skill, Investigation of the presence of an aliphatic biopolymer in cyanobacteria: implications for kerogen formation, Org. Geochem. 81 (2015) 64–69.

[6] M. Pathak, H. Kweon, M. Deo, H. Huang, Kerogen swelling and confinement: its implication on fluid thermodynamic properties in shales, Sci. Rep. 7 (2017) 12530–12543.

[7] A.R. Brandt, Converting oil shale to liquid fuels with the Alberta Taciuk processor: energy inputs and greenhouse gas emissions, Energ. Fuel 23 (2015) 6253–6258.

[8] P.M. Crawford, K. Biglarbigi, A. R. Dammer, E. Knaus, Advances in world oil-shale production technologies, in: SPE Annual Technical Conference and Exhibition, 21–24 September 2008, Denver, Colorado, USA, 2008.

[9] M.C. Branch, In-situ combustion retorting of oil shale, Prog. Energy Combust. Sci. 5 (1979) 193–206.

[10] N. Sullivan, G. Anyenya, B. Haun, M. Daubenspeck, J. Bonadies, R. Kerr, B. Fischer, A. Wright, G. Jones, R. Li, M. Wall, In-ground operation of Geothermic Fuel Cells for unconventional oil and gas recovery, J. Power Sources 302 (2016) 402–409.

[11] A. Brandt, Converting oil shale to liquid fuels: energy inputs and greenhouse gas emissions of the shell in-situ conversion process, Environ. Sci. Technol. 42 (2008) 7489–7495.

[12] W.A. Symington, D.L. Olgaard, G.A. Otten, T.C. Phillips, M.M. Thomas, J.D. Yeakel, ExxonMobil's electrofrac process for in-situ oil shale conversion, Proceedings of the AAPG Annual Convention, San Antonio, USA, April 20-23 2008, American Association of Petroleum Geologists, TX, USA, 2008, pp. 04–33.

[13] R. Carlson, E. Blase, T. McLendon, Development of the IIT Research Institute RF heating process for in-situ oil shale/tar sand fuel extraction – an overview, Proceedings of the 14th Oil Shale Symposium, Colorado School of Mines, Golden, USA, 1981, pp. 04–22.

[14] A. Bolonkin, J. Friedlander, S. Neumann, Strategic Solutions Technology Group, innovative unconventional oil extraction technologies, Fuel Process. Technol. 124 (2014) 228–242.

[15] J. Espitalié, K.S. Makadi, J. Trichet, Role of the mineral matrix during kerogen pyrolysis, Org. Geochem. 6 (1984) 365–382.

[16] M. Meslé, G. Dromart, F. Haeseler, P.M. Oger, Classes of organic molecules targeted by a methanogenic microbial consortium grown on sedimentary rocks of various maturities, Front. Microbiol. 6 (2015) Article Number: 589.

[17] J.H. Campbell, The Kinetics of Decomposition of Colorado Oil Shale II: Carbonate Minerals, Technical Report UCRL-52089 Part 2 Livermore, CA, Lawrence Livermore National Laboratory, 1978.

[18] S.R. Kelemen, H. Freund, M.L. Gorbaty, P.J. Kwiatek, Thermal chemistry of nitrogen in kerogen and low-rank coal, Energ. Fuel 13 (1999) 529–538.

[19] A. Aboulkas, K.E.I. Harfi, Effects of acid treatments on Moroccan Tarfaya oil shale and pyrolysis of oil shale and their kerogen, J. Fuel. Chem. Technol. 37 (2009) 659–667.

[20] A. Aboulkas, K.E.I. Harfi, Study of the kinetics and mechanisms of thermal decomposition of Moroccan Tarfaya oil shale and its kerogen, Oil Shale 25 (2008) 426–443.

[21] G.Đ. Gajica, A.M. Šajnović, K.A. Stojanović, M.D. Antonijević, N.M. Aleksić, B.S. Jovančićević, The influence of pyrolysis type on shale oil generation and its composition (Upper layer of Aleksinac oil shale, Serbia), J. Serb. Chem. Soc. 82 (2017) 1461–1477.

[22] P. Tiwari, M. Deo, Detailed kinetic analysis of oil shale pyrolysis TGA data, AIChE J. 58 (2012) 505–515.

[23] F. Behar, M. Vandenbroucke, Chemical modelling of kerogens, Org. Geochem. 11 (1987) 15–24.

[24] C.G. Scouten, M. Siskin, K.D. Rose, T. Aczel, S.G. Colgrove, R.E. Pabst Jr., Detailed structural characterization of the organic material in Rundle Ramsay crossing oil shale, Prepr. ACS Div. Petrol. Chem. 34 (1989) 43–47.

[25] M. Siskin, C.G. Scouten, K.D. Rose, T. Aczel, S.G. Colgrove, R.E. Pabst, Jr., in: C. Snape (Ed.), Detailed Structural Characterization of the Organic Material in Rundle Ramsay Crossing and Green River Oil Shales. Composition, Geochemistry and Conversion of Oil Shales, NATO ASI Series, vol 455 (Kluwer, 1995), pp. 143–158.

[26] A.M. Orendt, I.S.O. Pimienta, S.R. Badu, M.S. Solum, R.J. Pugmire, D.R. Locke, K.W. Chapman, P.J. Chupas, R.E. Winans, Three-dimensional structure of the Siskin Green River oil shale kerogen model: a comparison between calculated and observed properties, Energ. Fuel. 27 (2013) 702–710.

[27] S.R. Kelemen, M. Afeworki, M.L. Gorbaty, M. Sansone, P.J. Kwiatek, C.C. Walters, H. Freund, M. Siskin, A.E. Bence, D.G. Curry, M. Solum, R.J. Pugmire, M. Vandenbroucke, M. Leblond, F. Behar, Direct characterization of kerogen by X-ray and solid-state 13C nuclear magnetic resonance methods, Energy Fuel. 21 (2007) 1548–1561.

[28] Y. Sun, F. Bai, X. Lü, C. Jia, Q. Wang, M. Guo, Q. Li, W. Guo, Kinetic study of Huadian oil shale combustion using a multi-stage parallel reaction model, Energy 82 (2015) 705–713.

[29] A.K. Burnham, Oil evolution from a self-purging reactor: kinetic and composition at 2 °C/min and 2 °C/h, Energy Fuel. 5 (1991) 205–214.

[30] A.K. Burnham, M.F. Singleton, High-Pressure Pyrolysis of Green River Oil Shale. Geochemistry and Chemistry of Oil Shales, American Chemical Society, Washington DC, 1983, pp. 335–351.

[31] A.K. Burnham, J.A. Happe, On the mechanism of kerogen pyrolysis, Fuel 63 (1983) 1353–1356.

[32] J.O. Jaber, S.D. Probert, Non-isothermal thermogravimetry and decomposition kinetics of two Jordian oil shales under different processing conditions, Fuel Process. Technol. 63 (2000) 57–70.

[33] J.H. Campbell, G.H. Koskinas, N.D. Stout, Kinetics of oil generation from Colorado oil shale, Fuel. 57 (1978) 372–376.

[34] D.S. Thakur, H.E. Nuttal, Kinetics of pyrolysis of Moroccan oil shale by thermogravimetry, Ind. Eng. Chem. Process. Des. Dev. 26 (1987) 1351–1356.

[35] R.L. Braun, A.J. Rothman, Oil shale pyrolysis: kinetics and mechanism of oil production, Fuel 54 (1975) 129–131.

[36] A.K. Burnham, R.L. Braun, General kinetic model of oil shale pyrolysis, In Situ 9 (1985) 1–23.

[37] W. Wang, S. Li, T. Tan, Y. Ma, Pyrolysis kinetics of oil shale and its kerogen, Appl. Mech. Mater. 733 (2015) 236–240.

[38] A. Shawabkeh, K.S. Abdel Halim, O. Al-Ayed, Isoconversional methods for kinetic modeling of kerogen pyrolysis using TG data, Appl. Mech. Mater. 835 (2016) 299–307.

[39] P.H. Ungerer, R. Pelet, Extrapolation of the kinetics of oil and gas formation from laboratory experiments to sedimentary basins, Nature 327 (1987) 52–54.

[40] F. Bai, W. Guo, X. Lü, Y. Liu, M.Y. Guo, Q. Li, Y. Sun, Kinetic study on the pyrolysis behavior of Huadian oil Shale via non-isothermal thermogravimetric data, Fuel 146 (2015) 111–118.

[41] Q. Liu, X. Han, Q. Li, Y. Huang, X. Jiang, TG-DSC analysis of pyrolysis process of two Chinese oil shales, J. Therm. Anal. Calorim. 116 (2014) 511–517.

[42] P.T. Williams, N. Ahmad, Investigation of oil-shale pyrolysis processing conditions using thermogravimetric analysis, Appl. Energy 66 (2000) 113–133.

[43] F. Wang, X. Zeng, Y. Wang, H. Su, J. Yu, G. Xu, Non-isothermal coal char gasification with CO₂ in a micro fluidized bed reaction analyzer and a thermogravimetric analyzer, Fuel 164 (2016) 403–409.

[44] J. Yu, X. Zeng, J. Zhang, M. Zhong, G. Zhang, Y. Wang, G. Xu, Isothermal differential characteristics of gas-solid reaction in micro-fluidized bed reactor, Fuel 103 (2013) 29–36.

[45] F. Wang, X. Zeng, S. Geng, J. Yue, S. Tang, Y. Cui, J. Yu, G. Xu, Distinctive hydrodynamics of a micro fluidized bed and its application to gas-solid reaction analysis, Energy Fuel 32 (2017) 4096–4106.

[46] G.W. Wang, J.L. Zhang, J.G. Shao, K.J. Li, H.B Zuo, Investigation of non-isothermal and isothermal gasification process of coal char using different kinetic model, Int. J Min. Sci. Technol. 25 (2015) 15–21.

[47] B. Janković, The kinetic modeling of the non-isothermal pyrolysis of Brazilian oil shale: application of the Weibull probability mixture model, J. Petrol. Sci. Eng. 11 (2013) 25–36.

[48] M. Van de Velden, J. Baeyens, I. Boukis, Modeling CFB biomass pyrolysis reactors, Biomass Bioenergy 32 (2008) 128–139.

[49] A. Brems, J. Baeyens, J. Beerlandt, R. Dewil, Thermogravimetric pyrolysis of waste polyethylene-terephthalate and polystyrene: a critical assessment of kinetics modelling, Resour. Conserv. Recycl. 55 (2011) 772–781.

[50] S.M. Al-Salem, P. Lettieri, J. Baeyens, Kinetics and product distribution of end of life tyres (ELTs) pyrolysis: a novel approach in polyisoprene and SBR thermal cracking, J. Hazard. Mater. 172 (2009) 1690–1694.

[51] H.L. Friedman, Kinetics of thermal degradation of char-forming plastics from thermogravimetry. application to a phenol plastic, J. Polym. Sci. Part C 6 (1964) 183–195.

[52] A. Ortega, A simple and precise linear integral method for isoconversional data, Thermochim. Acta 474 (2008) 81–86.

[53] T. Ozawa, A new method of analyzing thermogravimetric data, Bull Chem. Soc. Jpn. 38 (1965) 1881–1886.

[54] S. Vyazovkin, D. Dollimore, Linear and nonlinear procedures in isoconversional computations of the activation energy of non-isothermal reactions in solids, J. Chem. Inf. Comput. Sci. 36 (1996) 42–45.

[55] P. Budrugeac, Differential non-linear isoconversional procedure for evaluating the activation energy of non-isothermal reactions, J. Therm. Anal. Calorim. 68 (2002) 131–139.

[56] C. Popescu, Integral method to analyze the kinetic of heterogeneous reactions under non-isothermal conditions: a variant on the Ozawa-Flynn-Wall method, Thermochim. Acta. 285 (1996) 309–323.

[57] J.M. Criado, Kinetic analysis of DTG data from master curves, Thermochim. Acta 24 (1978) 186–189.

[58] S. Vyazovkin, A.K. Burnham, J.M. Criado, L.A. Pérez-Maqueda, C. Popescu,

N. Sbirrazzuoli, ICTAC kinetics committee recommendations for performing kinetic computations on thermal analysis data, Thermochim. Acta 520 (2011) 1–19.

[59] J.L. Hillier, T. Bezzant, T.H. Fletcher, Improved Method for Determination of Kinetic Parameters from Non-isothermal TGA Data, Energy Fuel 24 (2010) 2841–2847.

[60] J.L. Hillier, T.H. Fletcher, Pyrolysis kinetics of a Green River oil shale using a pressurized TGA, Energy Fuel 25 (2011) 232–239.

[61] A. Khawam, D.R. Flanagan, Solid-state kinetic models: basics and mathematical fundamentals, J. Phys. Chem. B. 110 (2006) 17315–17328.

[62] A.K. Burnham, L.N. Dinh, A comparison of isoconversional and model-fitting approaches to kinetic parameter estimation and application predictions, J. Therm. Anal. Calorim. 89 (2007) 479–490.

[63] M.A. Galan, J.M. Smith, Pyrolysis of oil shale: experimental study of transport effects, AIChE J. 29 (1983) 604–610.

[64] E. Cheikh Moine, K. Groune, A.E.I. Hamidi, M. Khachani, M. Halim, S. Arsalane, Multistep process kinetics of the non-isothermal pyrolysis of Moroccan Rif oil shale, Energy 115 (2016) 931–941.

[65] A. Khawam, D.R. Flanagan, Basics and applications of solid-state kinetics: a pharmaceutical perspective, J. Pharm. Sci. 95 (2006) 472–498.

[66] M. Venkatesh, P. Ravi, S.P. Tewari, Isoconversional kinetic analysis of decomposition of nitroimidazoles: Friedman method vs Flynn-Wall-Ozawa method, J. Phys. Chem. A 117 (2013) 10162–10169.

[67] Z. Yuan, X. Chen, H. Xu, X. Qu, B. Wang, Crystallization kinetics of ultrafine $Co_{74.4}B_{25.6}$ amorphous powder prepared by chemical reduction, J. Alloy. Compd. 422 (2006) 109–115.

[68] P.E. Sánchez-Jiménez, L.A. Pérez-Maqueda, A. Perejón, J.M. Criado, Generalized master plots as a straightforward approach for determining the kinetic model: the case of cellulose pyrolysis, Thermochim. Acta 552 (2013) 54–59.

[69] J. Malek, Kinetic analysis of crystallization processes in amorphous materials, Thermochim. Acta 355 (2000) 239–253.

[70] J.M. Criado, L.A. Perez-Maqueda, F.J. Gotor, J. Malek, N. Koga, A unified theory for the kinetic analysis of solid state reactions under any thermal pathway, J. Therm. Anal. Calorim. 72 (2003) 901–906.

[71] A.W. Coats, J.P. Redfern, Kinetic parameters from thermogravimetric data, Nature 201 (1964) 68–69.

[72] C. Lu, W. Song, W. Lin, Kinetics of biomass catalytic pyrolysis, Biotechnol. Adv. 27 (2009) 583–587.

[73] D. Vamvuka, E. Kakaras, E. Kastanaki, P. Grammelis, Pyrolysis characteristics and kinetics of biomass residuals mixtures with lignite, Fuel 82 (2003) 1949–1960.

[74] A.M. Cortés, A.V. Bridgwater, Kinetic study of the pyrolysis of miscanthus and its acid hydrolysis residue by thermogravimetric analysis, Fuel. Process. Technol. 138 (2015) 184–193.

[75] D. Lai, J.H. Zhan, Y. Tian, S. Gao, G. Xu, Mechanism of kerogen pyrolysis in terms of chemical structure transformation, Fuel 119 (2017) 504–511.

[76] F. Hershkowitz, W.N. Olmstead, R.P. Rhodes, K.D. Rose, Molecular mechanism of oil shale pyrolysis in nitrogen and hydrogen atmospheres, Am. Chem. Soc. Symp. 281 (1983) 301–316.

[77] S. Li, C. Yue, Study of pyrolysis kinetic of oil shale, Fuel 82 (2003) 337–342.

[78] P.D. Garn, An examination of the kinetic compensation effect, J. Therm. Anal. 7 (1975) 475–478.

[79] Z. Gao, M. Nakada, I. Amasaki, A consideration of errors and accuracy in the isoconversional methods, Thermochim. Acta 369 (2001) 137–142.